The transfer between electron bulk kinetic energy and thermal energy in collisionless magnetic reconnection

San Lu, Quanming Lu, Can Huang, and Shui Wang

Citation: Phys. Plasmas **20**, 061203 (2013); doi: 10.1063/1.4811119
View online: http://dx.doi.org/10.1063/1.4811119
View Table of Contents: http://pop.aip.org/resource/1/PHPAEN/v20/i6
Published by the AIP Publishing LLC.

The transfer between electron bulk kinetic energy and thermal energy in collisionless magnetic reconnection

San Lu, Quanming Lu,[a] Can Huang, and Shui Wang
CAS Key Lab of Basic Plasma Physics, University of Science and Technology of China, Hefei 230026, China

(Received 15 July 2012; accepted 9 November 2012; published online 14 June 2013)

By performing two-dimensional particle-in-cell simulations, we investigate the transfer between electron bulk kinetic and electron thermal energy in collisionless magnetic reconnection. In the vicinity of the X line, the electron bulk kinetic energy density is much larger than the electron thermal energy density. The evolution of the electron bulk kinetic energy is mainly determined by the work done by the electric field force and electron pressure gradient force. The work done by the electron gradient pressure force in the vicinity of the X line is changed to the electron enthalpy flux. In the magnetic island, the electron enthalpy flux is transferred to the electron thermal energy due to the compressibility of the plasma in the magnetic island. The compression of the plasma in the magnetic island is the consequence of the electromagnetic force acting on the plasma as the magnetic field lines release their tension after being reconnected. Therefore, we can observe that in the magnetic island the electron thermal energy density is much larger than the electron bulk kinetic energy density. © *2013 AIP Publishing LLC*. [http://dx.doi.org/10.1063/1.4811119]

I. INTRODUCTION

Magnetic reconnection provides the fundamental mechanism in plasma for fast energy conversion from magnetic energy to plasma kinetic energy. During the reconnection process, magnetic energy is released and transferred to plasma kinetic energy.[1–4] The energy conversion is accompanied by topological changes of the magnetic field. Magnetic reconnection is considered to be associated with many explosive phenomena in solar atmosphere,[5–7] the Earth's magnetosphere,[8–10] laboratory experiments,[11–13] and even the magnetotail of non-magnetized planet.[14,15]

Plasma heating and acceleration are important signatures of magnetic reconnection. By performing two-dimensional (2-D) magnetohydrodynamic (MHD) simulations of magnetic reconnection, Birn and Hesse[16] studied the release and transfer of energy in the vicinity of the X line. It is found that magnetic energy (Poynting flux) is converted into both kinetic energy flux and enthalpy flux, and the kinetic energy flux becomes smaller with the increase of the guide field. The conversion of magnetic energy to enthalpy flux is considered to be stemmed mainly from the fact that the outflow occurs into a closed field governed by approximate force balance between Lorentz and pressure gradient forces.[16] Aunai *et al.*[17] further investigated ion energy budgets in collisionless anti-parallel magnetic reconnection with hybrid simulations. Magnetic energy loss is found to be not equally partitioned between ion thermal and ion bulk kinetic energies, and the ion thermal energy is favored.

The resistance provided by the classical collision rate in MHD theory can not explain fast reconnection rate required by explosive phenomena in plasma.[18] It is generally accepted that the Hall effect in collisionless plasma plays a critical role in the modeling of fast reconnection.[19–21] In the ion diffusion region of collisionless magnetic reconnection, electrons move along the separatrices until they reach the electron diffusion region, while ions are unmagnetized and can cross magnetic field lines.[19–23] The resulting Hall effect generates a quadrupolar structure of the out-of-plane magnetic field.[22–30] In the electron diffusion region, electrons are also unmagnetized and directed away from the X line along the magnetic field just inside the separatrices after they are accelerated by the reconnection electric field in the vicinity of the X line.[29,31,32] The reconnection electric field is considered to be determined mainly by the electron off-diagonal pressure tensor term.[33–38] Therefore, understanding of electron dynamics is the key to reveal the essence of collisionless magnetic reconnection. Figuring out the dissipation of magnetic energy into electron bulk kinetic energy and thermal energy is meaningful to understand the electron dynamics in collisionless reconnection. Despite its importance, electron energy transfer in magnetic reconnection is still unclear.

In this paper, the evolution of the electron bulk kinetic energy and thermal energy in both the vicinity of the X line and magnetic island is investigated. At the same time, a guide field is found to change electron dynamics significantly in collisionless magnetic reconnection,[29,31,32,39–44] and its influence on the transfer between electron bulk kinetic energy and thermal energy is also discussed in this paper.

In Sec. II, we will describe the 2-D particle-in-cell (PIC) model of our simulations. In Sec. III, the simulation results are presented. The conclusions and discussion will be stated in Sec. IV.

II. SIMULATION MODEL

In this paper, we use a 2-D PIC model to investigate the transfer between electron bulk kinetic energy and electron thermal energy in collisionless magnetic reconnection. In the model, the electromagnetic fields are defined on the grids and updated by solving the Maxwell equations with a full

[a]Author to whom correspondence should be addressed. Electronic mail: qmlu@ustc.edu.cn

explicit algorithm, and the ions and electrons are advanced in the electromagnetic field. The initial equilibrium configuration is a one-dimensional Harris current sheet in the (x, z) plane, where the initial magnetic field and the corresponding number density are given by[45]

$$\mathbf{B}_0(z) = B_0 \tanh(z/\delta)\mathbf{e}_x + B_{y0}\mathbf{e}_y, \quad (1)$$

$$n(z) = n_b + n_0 \sec \mathrm{h}^2(z/\delta), \quad (2)$$

where B_0 is the asymptotical magnitude of the magnetic field, δ is the half-width of the current sheet, and B_{y0} is the initial guide field. n_b is the number density of the background plasma, and n_0 is the peak Harris number density. At the same time, the initial distribution functions for the ions and electrons are Maxwellian with drift speeds in the y direction, which satisfy the equation $V_{i0}/V_{e0} = -T_{i0}/T_{e0}$ (where $V_{i0}(V_{e0})$ and $T_{i0}(T_{e0})$ are the initial drift speed and temperature of ions(electrons), respectively). In our simulations, we set $T_{i0}/T_{e0} = 4$ and $n_b = 0.2n_0$. The initial half-width of the Harris current sheet is $\delta = 0.5c/\omega_{pi}$, where c/ω_{pi} is the ion inertial length defined by n_0. The mass ratio m_i/m_e is chosen to be 100. The light speed is $c = 15v_A$, where v_A is the Alfven speed based on B_0 and n_0.

The computation is carried out in a rectangular domain in the (x, z) plane with the dimension $L_x \times L_z = (12.8c/\omega_{pi}) \times (6.4c/\omega_{pi})$. The grid number is $N_x \times N_z = 256 \times 128$. Therefore, the simulation spatial resolution is $\Delta x = \Delta z = 0.05c/\omega_{pi} = 0.5c/\omega_{pe}$. The time step is $\Omega_i t = 0.001$, where $\Omega_i = eB_0/m_i$ is the ion gyrofrequency. We employ more than 5×10^7 particles per species to simulate the plasma. The periodic boundary conditions are used along the x direction; at the same time, ideal conducting boundary conditions for the electromagnetic fields and reflected boundary conditions for particles are used in the z direction. In order to make the system enter the nonlinear stage quickly, the initial current sheet is modified, as in the Geospace Environmental Modeling (GEM) Challenge reconnection problem,[16] by including an initial flux perturbation.

III. SIMULATION RESULTS

We perform 2-D PIC simulations to investigate the transfer between electron bulk kinetic energy and electron thermal energy in collisionless magnetic reconnection. The electron bulk kinetic energy density and thermal energy density are defined as $K_e = \frac{1}{2}n_e m_e(V_{ex}^2 + V_{ey}^2 + V_{ez}^2)$ (where n_e is the electron number density and V_{ex}, V_{ey}, V_{ez} are the electron bulk velocities in the x, y, z direction) and $u_e = \frac{1}{2}n_e k(T_{ex} + T_{ey} + T_{ez})$ (where T_{ex}, T_{ey}, T_{ez} are the electron temperatures in the x, y, and z directions), respectively.

The time evolution of the electron bulk kinetic energy density is governed by

$$\frac{\partial K_e}{\partial t} = -\nabla \cdot (K_e \mathbf{V}_e) - n_e e \mathbf{V}_e \cdot \mathbf{E} - (\nabla \cdot \bar{\mathbf{P}}_e) \cdot \mathbf{V}_e, \quad (3)$$

where $\mathbf{V}_e$ is the electron bulk velocity, $\mathbf{E}$ is the electric field, and $\bar{\mathbf{P}}_e$ denotes the electron pressure tensor. The first term in the right-hand-side (RHS) of Eq. (3) is the divergence of the electron bulk kinetic energy flux. The last two terms in the RHS are the power densities of the work done by electric field force and electron pressure gradient force, which act as the electron bulk kinetic energy source terms.

Electron thermal energy evolution can be described as

$$\frac{\partial u_e}{\partial t} = -\nabla \cdot \mathbf{Q}_e - \nabla \cdot \mathbf{H}_e + \mathbf{V}_e \cdot (\nabla \cdot \bar{\mathbf{P}}_e), \quad (4)$$

where $\mathbf{H}_e = u_e \mathbf{V}_e + \bar{\mathbf{P}}_e \cdot \mathbf{V}_e$ is the electron enthalpy flux density. $\mathbf{Q}_e = \frac{1}{2}m_e \int (\mathbf{v} - \mathbf{V}_e)^2 (\mathbf{v} - \mathbf{V}_e) f_e d\mathbf{v}$ is the electron heat flux, which is associated with the asymmetric electron velocity distribution (where f_e is the electron velocity distribution). The RHS terms of Eq. (4) are the divergence of the electron heat flux, the divergence of the electron enthalpy energy flux density, and the power density of the work done by electron pressure gradient force, respectively.

Figure 1 shows the electron bulk kinetic energy density for (a) $B_{y0} = 0$ at $\Omega_i t = 16.5$ and (b) $B_{y0} = B_0$ at $\Omega_i t = 21$. The time is selected when the maximum reconnection rates are attained. In both cases, the electron bulk kinetic energy density in the vicinity of the X line is much larger than that in the other region. This phenomenon is more obvious in the case $B_{y0} = B_0$. The maximum values of the electron bulk kinetic energy density are about 0.01 and 0.03 $n_0 m_i v_A^2$ for the cases $B_{y0} = 0$ and $B_{y0} = B_0$, respectively.

Figure 2 shows the electron thermal energy density for (a) $B_{y0} = 0$ at $\Omega_i t = 16.5$ and (b) $B_{y0} = B_0$ at $\Omega_i t = 21$. Note that in the simulations, we use periodic boundary condition. Therefore, the magnetic field lines are closed around the denoted region by the black rectangle in the figure, where a magnetic island is formed. Obviously, in both cases, the electron thermal energy density in the magnetic island is much higher than that in the other region. This phenomenon

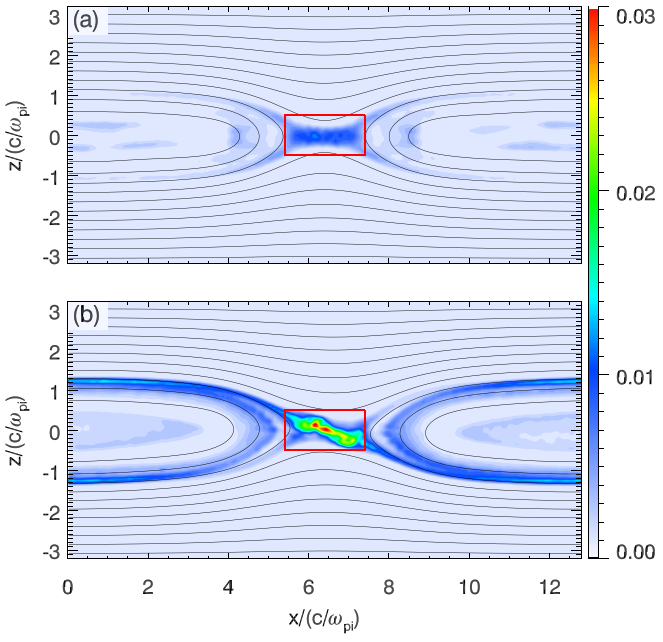

FIG. 1. Contours of the electron bulk kinetic energy density for the cases (a) $B_{y0} = 0$ at $\Omega_i t = 16.5$ and (b) $B_{y0} = B_0$ at $\Omega_i t = 21$. In the figure, the magnetic field lines are also plotted for reference. The electron bulk kinetic energy density is normalized by $n_0 m_i v_A^2$.

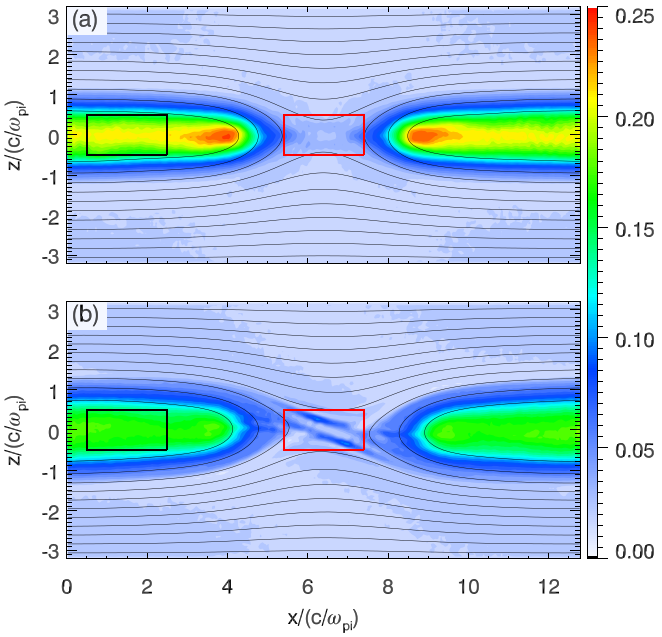

FIG. 2. Contours of the electron thermal energy density for the cases (a) $B_{y0} = 0$ at $\Omega_i t = 16.5$ and (b) $B_{y0} = B_0$ at $\Omega_i t = 21$. In the figure, the magnetic field lines are also plotted for reference. The electron bulk kinetic energy density is normalized by $n_0 m_i v_A^2$.

is more obvious in the case $B_{y0} = 0$. In the magnetic island, the maximum values of the electron thermal energy density are about 0.21 and 0.15 $n_0 m_i v_A^2$ for the cases $B_{y0} = 0$ and $B_{y0} = B_0$, respectively.

In order to demonstrate the time evolution of the electron bulk kinetic energy more clearly, we integrate the RHS terms of Eq. (3) in the selected region which has been denoted by the red rectangles in Figs. 1 and 2. Figure 3 shows their time evolutions for (a) $B_{y0} = 0$ and (b) $B_{y0} = B_0$. In both cases the contribution of the electron bulk kinetic energy flux is much smaller than the other two terms. The main difference is the contribution of the work done by the electron pressure gradient force, whose net effect is to reduce the electron bulk kinetic energy. In the vicinity of the X line,

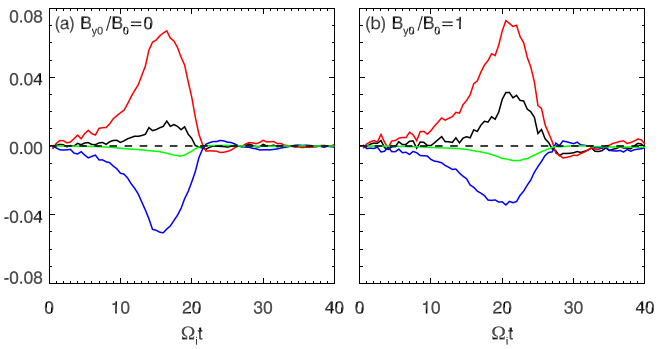

FIG. 3. Time evolutions of the right-hand-side terms of Eq. (3) integrated in the selected region denoted with red rectangles (in the vicinity of the X line) in Figs. 1 and 2 for the cases (a) $B_{y0} = 0$ and (b) $B_{y0} = B_0$, respectively. The green curve represents the electron bulk kinetic energy flux term $-\int \nabla \cdot (K_e \mathbf{V}_e) dxdz$, the red curve denotes the power density of the work done by the electric field $-\int n_e e \mathbf{V}_e \cdot \mathbf{E} dxdz$, and the power density of the work done by the electron pressure gradient $-\int (\nabla \cdot \bar{\mathbf{P}}_e) \cdot \mathbf{V}_e dxdz$ is described by the blue curve. The black curves are the sums of the three terms. All these terms are normalized by $n_0 m_i v_A^2 \Omega_i \Delta x \Delta z$.

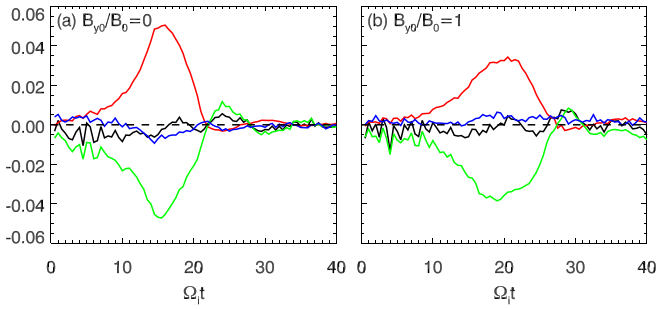

FIG. 4. Time evolutions of the right-hand-side terms of Eq. (4) integrated in the selected region denoted by red rectangles (in the vicinity of the X line) in Figs. 1 and 2 for the cases (a) $B_{y0} = 0$ and (b) $B_{y0} = B_0$. The green, blue, and red curves represent the electron enthalpy flux term $-\int \nabla \cdot \mathbf{H}_e dxdz$, the electron heat flux term $-\int \nabla \cdot \mathbf{Q}_e dxdz$, and the thermal energy source term $\int (\nabla \cdot \bar{\mathbf{P}}_e) \cdot \mathbf{V}_e dxdz$, respectively. The black curves are the sums of the three terms. All these terms are normalized by $n_0 m_i v_A^2 \Omega_i \Delta x \Delta z$.

the work done by the electron pressure gradient force in the case $B_{y0} = 0$ is larger than that in the case $B_{y0} = B_0$, which leads to the larger electron bulk kinetic energy in the case $B_{y0} = B_0$. We also integrate the RHS terms of Eq. (4) in the selected region denoted in Figs. 1 and 2 with red rectangles, and Figure 4 shows their time evolutions. The electron thermal energy as well as its temporal derivative is very small in the vicinity of the X line. The work done by the electron pressure gradient force is changed to the electron enthalpy flux.

For a further investigation of the high electron thermal energy inside the magnetic island, especially in the case $B_{y0} = 0$, we hereafter integrate the RHS terms of Eq. (4) in the selected region denoted in Fig. 2 with black rectangles inside the magnetic island, and the time evolutions for both cases are shown in Fig. 5. In both cases, inside the magnetic island, the work done by the electron pressure gradient force and the electron heat flux are small and negligible, and the increase of the electron thermal energy is controlled by the electron enthalpy flux. In the vicinity of the X line, the plasma is accelerated by the reconnection electric field and leaves this region, which then compresses the plasma in the magnetic island. In the magnetic island, the compression of the magnetic island leads to the electron enthalpy flux into

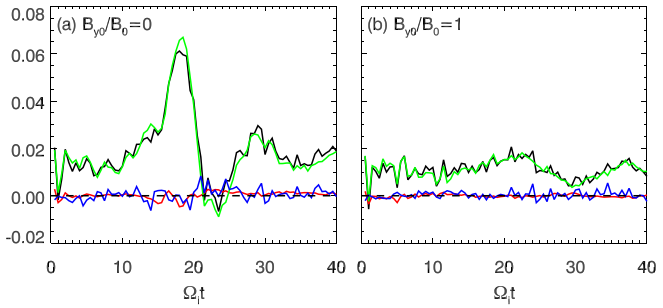

FIG. 5. Time evolutions of the right-hand-side terms of Eq. (4) integrated in the selected region denoted by black rectangles (in the magnetic island) in Fig. 2 for the cases (a) $B_{y0} = 0$ and (b) $B_{y0} = B_0$. The green, blue, and red curves represent the electron enthalpy flux term $-\int \nabla \cdot \mathbf{H}_e dxdz$, the electron heat flux term $-\int \nabla \cdot \mathbf{Q}_e dxdz$, and the thermal energy source term $\int (\nabla \cdot \bar{\mathbf{P}}_e) \cdot \mathbf{V}_e dxdz$, respectively. The black curves are the sums of the three terms. All these terms are normalized by $n_0 m_i v_A^2 \Omega_i \Delta x \Delta z$.

the electron thermal energy. The existence of the initial guide field will lower the compressibility of the plasma in the magnetic island; therefore, the electron enthalpy flux into the magnetic island in the case $B_{y0} = 0$ is much larger than that in the case $B_{y0} = B_0$, which causes the larger electron thermal energy in the island.

IV. CONCLUSIONS

In this paper, using 2-D PIC simulations, we investigate the transfer between electron bulk kinetic and thermal energy in collisionless magnetic reconnection. The electron bulk kinetic energy and electron thermal energy is concentrated in the vicinity of the X line and the magnetic island, respectively. In the vicinity of the X line, the increase of the electron bulk kinetic energy is dominated by the work done by the electric field force and electron gradient pressure force, while the electron thermal energy is negligible. The work done by the electron gradient pressure force in the vicinity of the X line is changed to the electron enthalpy flux, which leaves the vicinity of the X line. In the magnetic island, the electron enthalpy flux is changed to the electron thermal energy due to the compression of the plasma in the magnetic island, which is the consequence of the electromagnetic force acting on the plasma as the magnetic field lines release their tension after being reconnected. Therefore, we can observe the increase of the electron thermal energy in the magnetic island. With the increase of the initial guide field, the compressibility of the magnetic island decreases, and there will be less electron enthalpy flux into the magnetic island. As a result, we can observe the smaller electron thermal energy in the magnetic island during guide field reconnection.

In magnetic reconnection, magnetic energy loss is found to be not equally partitioned between ion thermal and bulk kinetic energies, and the thermal energy is favored.[17] Similar situation also applies to the electrons, the increase of the electron bulk kinetic energy and electron thermal energy in magnetic reconnection is shown in Table I. Obviously, the electron bulk kinetic energy and electron thermal energy are not equally partitioned, and the electron thermal energy is favored. With the continuous increase of the initial guide field, the obtained electron thermal energy during reconnection becomes less and less important. It is easy to understand that with the increase of the guide field, the plasma in the magnetic island becomes less compressive and harder to be heated. Also note that the ratio between the ion kinetic energy gain and the electron kinetic energy gain is approximately constant and about 3 in our simulations. However, the ratio will change with the variations of the mass ratio between ion and electron. Electron heating and acceleration are important signatures in many explosive phenomena related to magnetic reconnection, and the significance of our results in these phenomena need further investigation.

TABLE I. The difference in the ion and electron kinetic energy in magnetic reconnection. ε_i denotes the ion kinetic energy (it includes the ion bulk kinetic energy and ion thermal energy), and ε_e denotes the electron kinetic energy (it includes the electron bulk kinetic energy and electron thermal energy). The electron bulk kinetic energy is denoted by ε_{be}, and the electron thermal energy is denoted by ε_{the}. "D" means the energy difference, which is calculated by subtracting the energy, when the reconnection attains its maximum rate, to its initial value. The energy is integrated over the entire simulation domain, and it is normalized by $n_0 m_i v_A^2 (c/\omega_{pi})^2$. An approximate conservation of the total energy is kept in our simulation models, and the percentage of energy non-conservation is within 0.4%.

B_{y0}/B_0	$D\varepsilon_i$	$D\varepsilon_e$	$D\varepsilon_{be}/D\varepsilon_e$ (%)	$D\varepsilon_{the}/D\varepsilon_e$ (%)
0	862.701	260.571	6.65	93.35
0.2	963.652	263.688	7.65	92.35
0.4	863.75	229.021	10.31	89.69
0.6	889.161	247.264	14.22	85.78
0.8	608.464	186.328	19.04	80.96
1	576.914	198.615	22.18	77.82

ACKNOWLEDGMENTS

This work was supported by the National Science Foundation of China (NSFC) under Grant Nos. 41174124 and 41121003, 973 Program (2013CBA01503, 2012CB825602), Ocean Public Welfare Scientific Research Project, State Oceanic Administration People's Republic of China (No. 201005017), and the Fundamental Research Funds for the Central Universities (WK2080000010).

[1]J. Birn and E. R. Priest, *Reconnection of Magnetic Fields: Magnetohydrodynamics and Collisionless Theory and Observations* (Cambridge University Press, Cambridge, 2007).
[2]D. Biskamp, *Magnetic Reconnection in Plasmas* (Cambridge University Press, Cambridge, 2000).
[3]V. M. Vasyliunas, Rev. Geophys. **13**, 303, doi:10.1029/RG013i001p00303 (1975).
[4]M. Yamada, R. Kulsrud, and H. T. Ji, Rev. Mod. Phys. **82**, 603 (2010).
[5]R. G. Giovanelli, Nature (London) **158**, 81 (1946).
[6]S. Masuda, T. Kosugi, H. Hara, and Y. Ogawara, Nature (London) **371**, 495 (1994).
[7]H. Q. Song, Y. Chen, G. Li, X. L. Kong, and S. W. Feng, Phys. Rev. X **2**, 021015 (2012).
[8]V. Angelopoulos, J. P. McFadden, D. Larson, C. W. Carlson, S. B. Mende, H. Frey, T. Phan, D. G. Sibeck, K. H. Glassmeier, U. Auster, E. Donovan, I. R. Mann, I. J. Rae, C. T. Russell, A. Runov, X. Z. Zhou, and L. Kepko, Science **321**, 931 (2008).
[9]D. N. Baker, T. I. Pulkkinen, V. Angelopoulos, W. Baumjohann, and R. L. McPherron, J. Geophys. Res. **101**, 12975, doi:10.1029/95JA03753 (1996).
[10]T. Nagai, M. Fujimoto, Y. Saito, S. Machida, T. Terasawa, R. Nakamura, T. Yamamoto, T. Mukai, A. Nishida, and S. Kokubun, J. Geophys. Res. **103**, 4419, doi:10.1029/97JA02190 (1998).
[11]H. T. Ji, M. Yamada, S. Hsu, and R. Kulsrud, Phys. Rev. Lett. **80**, 3256 (1998).
[12]C. K. Li, F. H. Seguin, J. A. Frenje, J. R. Rygg, R. D. Petrasso, R. P. J. Town, O. L. Landen, J. P. Knauer, and V. A. Smalyuk, Phys. Rev. Lett. **99**, 055001 (2007).
[13]Q. L. Dong, S. J. Wang, Q. M. Lu, C. Huang, D. W. Yuan, X. Liu, X. X. Lin, Y. T. Li, H. G. Wei, J. Y. Zhong, J. R. Shi, S. E. Jiang, Y. K. Ding, B. B. Jiang, K. Du, X. T. He, M. Y. Yu, C. S. Liu, S. Wang, Y. J. Tang, J. Q. Zhu, G. Zhao, Z. M. Sheng, and J. Zhang, Phys. Rev. Lett. **108**, 215001 (2012).
[14]J. P. Eastwood, D. A. Brain, J. S. Halekas, J. F. Drake, T. D. Phan, M. Oieroset, D. L. Mitchell, R. P. Lin, and M. Acuna, Geophys. Res. Lett. **35**, L02106, doi:10.1029/2007GL032289 (2008).
[15]T. L. Zhang, Q. M. Lu, W. Baumjohann, C. T. Russell, A. Fedorov, S. Barabash, A. J. Coates, A. M. Du, J. B. Cao, R. Nakamura, W. L. Teh, R. S. Wang, X. K. Dou, S. Wang, K. H. Glassmeier, H. U. Auster, and M. Balikhin, Science **336**, 567 (2012).
[16]J. Birn and M. Hesse, Phys. Plasmas **17**, 012109 (2010).
[17]N. Aunai, G. Belmont, and R. Smets, Phys. Plasmas **18**, 122901 (2011).

[18]D. Biskamp, Phys. Fluids **29**, 1520 (1986).
[19]J. Birn, J. F. Drake, M. A. Shay, B. N. Rogers, R. E. Denton, M. Hesse, M. Kuznetsova, Z. W. Ma, A. Bhattacharjee, A. Otto, and P. L. Pritchett, J. Geophys. Res. **106**, 3715, doi:10.1029/1999JA900449 (2001).
[20]M. A. Shay, J. F. Drake, B. N. Rogers, and R. E. Denton, J. Geophys. Res. **106**, 3759, doi:10.1029/1999JA001007 (2001).
[21]J. F. Drake, M. A. Shay, and M. Swisdak, Phys. Plasmas **15**, 042306 (2008).
[22]B. U. Ö. Sonnerup, "Magnetic field reconnection," in *Solar System Plasma Physics*, edited by L. J. Lanzèrotti, C. F. Kennel, and E. N. Parker (North-Holland, New York, 1979), Vol. 3, p. 46.
[23]R. S. Wang, Q. M. Lu, C. Huang, and S. Wang, J. Geophys. Res. **115**, A01209, doi:10.1029/2009JA014553 (2010).
[24]P. L. Pritchett, J. Geophys. Res. **106**, 3783, doi:10.1029/1999JA001006 (2001).
[25]T. Nagai, I. Shinohara, M. Fujimoto, M. Hoshino, Y. Saito, S. Machida, and T. Mukai, J. Geophys. Res. **106**, 25929, doi:10.1029/2001JA900038 (2001).
[26]Z. W. Ma and A. Bhattacharjee, J. Geophys. Res. **106**, 3773, doi:10.1029/1999JA001004 (2001).
[27]B. N. Rogers, R. E. Denton, and J. F. Drake, J. Geophys. Res. **108**, 1111, doi:10.1029/2002JA009699 (2003).
[28]A. Runov, R. Nakamura, W. Baumjohann, R. A. Treumann, T. L. Zhang, M. Volwerk, Z. Voros, A. Balogh, K. H. Glassmeier, B. Klecker, H. Reme, and L. Kistler, Geophys. Res. Lett. **30**, 1579, doi:10.1029/2002GL016730 (2003).
[29]X. R. Fu, Q. M. Lu, and S. Wang, Phys. Plasmas **13**, 012309 (2006).
[30]Q. M. Lu, C. Huang, J. L. Xie, R. S. Wang, M. Y. Wu, A. Vaivads, and S. Wang, J. Geophys. Res. **115**, A11208, doi:10.1029/2010JA015713 (2010).
[31]P. L. Pritchett, Geophys. Res. Lett. **33**, L13104, doi:10.1029/2005GL025267 (2006).
[32]C. Huang, Q. M. Lu, and S. Wang, Phys. Plasmas **17**, 072306 (2010).
[33]H. J. Cai, D. Q. Ding, and L. C. Lee, J. Geophys. Res. **99**, 35, doi:10.1029/93JA02519 (1994).
[34]H. J. Cai and L. C. Lee, Phys. Plasmas **4**, 509 (1997).
[35]M. Hesse and D. Winske, J. Geophys. Res. **103**, 26479, doi:10.1029/98JA01570 (1998).
[36]M. Hesse, K. Schindler, J. Birn, and M. Kuznetsova, Phys. Plasmas **6**, 1781 (1999).
[37]M. Hesse, M. Kuznetsova, and M. Hoshino, Geophys. Res. Lett. **29**, 1563, doi:10.1029/2001GL014714 (2002).
[38]W. G. Wan, G. Lapenta, G. L. Delzanno, and J. Egedal, Phys. Plasmas **15**, 102302 (2008).
[39]M. Hesse, M. Kuznetsova, K. Schindler, and J. Birn, Phys. Plasmas **12**, 100704 (2005).
[40]P. Ricci, J. U. Brackbill, W. Daughton, and G. Lapenta, Phys. Plasmas **11**, 4102 (2004).
[41]P. Ricci, G. Lapenta, and J. U. Brackbill, Phys. Plasmas **10**, 3554 (2003).
[42]P. L. Pritchett, Phys. Plasmas **12**, 062301 (2005).
[43]P. L. Pritchett, J. Geophys. Res. **111**, A10212, doi:10.1029/2006JA011793 (2006).
[44]P. L. Pritchett and F. V. Coroniti, J. Geophys. Res. **109**, A01220, doi:10.1029/2003JA009999 (2004).
[45]E. G. Harris, Nuovo Cimento **23**, 115 (1962).